scientific reports

OPEN

Hyperspectral analysis and inversion model study of water content in magnetite

Yang Bai[1], Xiaoxiao Xie[2✉], Jiuling Zhang[2], Yuna Jia[1] & Handi Wang[3]

Excessive moisture in iron ore hinders pulverization, beneficiation, and smelting. Traditional detection methods struggle with complex ore compositions. This study developed a hyperspectral model to estimate moisture in Hebei magnetite. Samples were preprocessed using S-G smoothing, MSC, SNV, derivatives, and continuum removal. CARS selected optimal bands, while PSO-LSSVR improved modeling. Reflectance showed a negative correlation with moisture, with Fe^{3+} (990 nm) and -OH (1440/1920 nm) absorption features. The models achieved R^2 values of 0.798 and 0.648. The integrated approach outperformed conventional methods, enabling accurate moisture detection for industrial use.

Keywords Hyperspectrum, Magnetite, Water content, Inversion model

With the promotion of intelligent mining policies, hyperspectral technology has become an important research focus in iron ore identification[1]. The water content of iron ore plays a critical role in ensuring product quality and production stability in mineral processing[2]. However, the complexity of production processes and the limited accuracy of traditional methods make rapid and precise moisture detection in iron ore challenging. Therefore, advancing modern identification technologies is essential to meet mining production demands.

Hyperspectral technology has attracted growing attention for its rapid, non-destructive detection of water content. In agriculture, researchers have leveraged its advantages to develop spectral models for moisture estimation, achieving promising predictive results[3–5]. In soil moisture prediction, model optimization improves both predictive accuracy and overall model efficiency[6–8]. Wang et al.[9] used infrared spectroscopy to analyze the spectral characteristics of sandstone and develop a moisture inversion model. They found that the absorption peaks near 1400 nm and 1900 nm were positively correlated with water content in the near-infrared spectra. Xu et al.[10] found that the spectral reflectance of tuff decreases progressively as water content increases. Zhang et al.[11] found that the absorption intensity near 1400 nm and 1900 nm was positively correlated with rock moisture content. However, research on mineral moisture detection remains limited. Bai et al.[12] conducted in-depth research on zinc ores with different water contents, revealing that the water content has a linear influence on the spectrum. Gao et al.[13] explored the water content of sinter by laser-induced breakdown spectroscopy, and found that there is a significant linear relationship between the water content and the average spectral intensity. Maurais J[14] employed spectral technology to monitor water content changes in tailings, revealing a clear correlation between spectral reflectance and moisture. The spectral features of evaporation residue effectively indicated surface drying rates. However, research on iron ore moisture is still limited, with room for improving model accuracy.

Hebei iron ore, with its large reserves and uniform composition, is ideal for producing high-quality steel. However, moisture in magnetite generates steam during smelting, affecting efficiency and safety. This study focuses on Anshan-type magnetite (38% grade), designing 20 moisture levels (0–40%) across 9 particle sizes. After spectral pretreatment, characteristic bands were selected using competitive adaptive reweighting, and moisture prediction models were developed using random forest regression, least squares support vector regression (LSSVR), and particle swarm optimized LSSVR. The models' accuracy and errors were compared to identify the optimal model for rapid, accurate moisture detection, enabling real-time monitoring during smelting. There are still some shortcomings in this study, such as the relatively single type of ore studied. However, in terms of novelty, compared to previous studies that focused on tailings or limited ore types, there are few studies that involve predicting the moisture content of magnetite with comprehensive particle size changes.

[1]College of Mining Engineering, North China University of Science and Technology, Tangshan 063210, China. [2]School of Emergency Management and Safety Engineering, North China University of Science and Technology, Tangshan 063210, China. [3]China Minmetals Group (Tangshan Caofeidian) Ore Holdings Co.,Ltd, Tangshan 063000, China. ✉email: xiaoxiaoxie415@stu.ncst.edu.cn

Fig. 1. Experimental flow chart: (**a**) magnetite collection, (**b**) magnetite sample treatment and saturation measurement, (**c**) magnetite spectrum experimental test.

Number	Water content (%)	Number	Water content (%)
1	0	11	21.0
2	3.0	12	24.0
3	5.0	13	25.0
4	6.0	14	28.0
5	9.0	15	30.0
6	10.0	16	31.0
7	12.0	17	33.0
8	15.0	18	35.0
9	18.0	19	38.0
10	20.0	20	40.0

Table 1. Water content grade of the samples.

This study combines advanced preprocessing, feature selection, and optimization algorithms to provide higher accuracy and wider applicability for industrial applications.

Experiments and methods

Sample collection and processing

Magnetite from a certain area in Hebei Province, China is selected as the experimental sample, with a grade of about 38% and the main component of Fe_3O_4, as shown in Fig. 1(a). The samples were crushed by a ball mill, and nine kinds of particle sizes (particle size 1: < 0.045 mm, particle size 2: 0.045–0.075 mm, particle size 3: 0.075–0.1 mm, particle size 4: 0.1–0.15 mm, particle size 5: 0.15–0.3 mm, particle size 6:0.3–0.5 mm, particle size 7:0.5–2 mm, particle size 8: 2–3 mm, particle size 9: >3 mm) were selected by standard screening. Before the experiment, slowly add water to the magnetite powder to ensure that the free water on its surface disappears completely, and then measure the saturation, and calculate that the saturation of the magnetite powder tends to 35.0%, as shown in Fig. 1(b). Based on this, 20 water content grades between 0% and 40% were designed to simulate magnetite samples under different humidity conditions to study the relationship between their spectral characteristics and water content. The water content grades are shown in Table 1.

Hyperspectral measurement of water content in magnetite

The water content spectrum of magnetite samples is measured by a portable ground object spectrometer (FieldSpec4) produced by Analytical Spectral Devices Company of the United States, and its spectral range is 350–2500 nm. The experiment was carried out in dark and dark environment to reduce the interference of external light on spectral measurement. After fully shaking the prepared mineral powder sample, put it in a black light-proof box. The water content of samples was determined by evaporation method at intervals to obtain

samples with different water content grades. In the process of spectral measurement, the lens of the spectrometer illuminates the sample vertically at 90 degrees, and 10 spectral curves are collected repeatedly, and the average value is taken as the original data. The experimental measurement process of the spectrum is shown in Fig. 1(c). Because the data in 350–399 nm and 2401–2500 nm bands are noisy and have low stability[15], only the spectral data in 400–2400 nm band are selected for data analysis and modeling.

Correlation analysis between spectral data preprocessing and pearson

Pretreatment of hyperspectral data can improve the accuracy and stability of the water content spectrum of magnetite to a certain extent[16], and S-G smoothing filtering (S-G), Multiple Scattering Correction, MSC), Standard Normal Transform (SNV), Second Derivative, SD), Logarithm Reciprocal, LR) and Continuum-Removal, CR) are used to transform the original spectrum. Pearson correlation coefficient is used to analyze the correlation between the water content of magnetite and the reflectivity of different data transformations, and the significance of the correlation coefficient is tested at the level of $P = 0.01$ to analyze the influence of spectral transformation on the prediction of the water content of magnetite.

Competitive adaptive weighting algorithm (CARS) for optimizing characteristic band

The hyperspectral data of water content in magnetite have the characteristics of strong band continuity and miscellaneous spectral information, and there are multiple collinearities between bands. In order to reduce data redundancy, the CARS algorithm is used to optimize features. CARS algorithm is based on the Monte Carlo sampling method and partial least squares regression model (PLSR) to select the characteristic wavelength. By using the exponential decay function and adaptive weighted sampling to calculate the weight of the absolute value of the regression coefficient, the wavelength variables with large weight and small collinearity are combined into a new subset of variables, and the band corresponding to PLSR model with minimum root mean square error of cross-validation is selected as the final characteristic band, to improve spectral data processing efficiency, reduce information redundancy and enhance the accuracy of ground object recognition[17].

Construction and accuracy evaluation of water content prediction model

Random Forest Regression (RFR), Least Squares Support Vector Regression (LSSVR) and Particle Swarm Optimization Least Squares Support Vector Regression (PSO-LSSVR) are used to predict the water content of magnetite. Random forest regression (RFR) model constructs multiple regression trees by random sampling, and synthesizes the weighted average results of these trees as the final prediction. The RFR model can effectively capture the complex nonlinear relationship between independent variables and dependent variables, and is suitable for high-dimensional data processing. The model performance can be optimized by adjusting the number of decision trees and the number of feature splits[18]. Least square support vector regression (LSSVR) is an alternative algorithm based on support vector (SVM), which has a perfect theoretical framework and transforms quadratic optimization problems into the solution process of linear equations, thus simplifying the solution of problems[19]. Particle Swarm Optimization Least Squares Support Vector Regression (PSO-LSSVR) is an advanced method combining Particle Swarm Optimization (PSO) and Least Squares Support Vector Regression (LSSVR). This method uses particle swarm optimization to optimize the superparameter selection of LSSVR and improve the performance and prediction accuracy of the model. The particles move in the search space, approach the target through continuous iteration, and finally converge to the optimal solution, which effectively reduces the risk of the model falling into local optimization[20].

In the hyperspectral modeling, the Random Forest (RF) model was configured with 100 decision trees to balance accuracy and computational efficiency. For the Particle Swarm Optimization (PSO) algorithm, a population size of 30 particles was used, which provided stable convergence and effective parameter optimization for the LSSVR model. The calibration set and the prediction set are randomly divided by the ratio of 3:1, and the training set and the test set are divided respectively for 200 samples with 9 granularity levels. The number of training set samples accounts for about 75% of the total sample, with 150 training set samples, and the remaining 50 samples are test set samples, which ensures the rationality and reliability of training set model establishment and test set verification. Taking the determining coefficient (R^2) and Root Mean Squared Erro (RMSE) as evaluation indexes, the closer the R^2 value is to 1 and the smaller the RMSE value, the better the stability and applicability of the model.

Based on the above description of the experimental process and analysis methods, the method flowchart of this study is shown in Fig. 2.

Results and discussion
Spectral curve characteristics of magnetite with different water content

The reflection spectra of magnetite with different water contents are shown in Fig. 3. The spectral curves of magnetite with different particle sizes are almost the same, and the reflectivity ranges from 0 to 0.03. With the increase of particle size, the reflectivity shows a downward trend, and the two are negatively correlated. The water content has a certain influence on the spectral characteristics of magnetite. With the increase of water content of magnetite, the overall reflectivity tends to decrease. However, the water content has little influence on the overall shape and trend of magnetite reflection spectrum curve. The spectral reflectance of magnetite has obvious absorption characteristics at 990 nm, 1440 nm and 1920 nm, and the absorption characteristic at 990 nm is the absorption band of Fe^{3+}, which is determined by the properties of magnetite. The absorption characteristics at 1440 nm and 1920 nm are influenced by -OH bond. The spectral curves of magnetite with different water contents decrease in the range of 400–500 nm, and gradually increase in the range of 500–600 nm, forming a weak trough near 500 nm, which is characterized by weak absorption due to the influence of Fe^{3+}. In the range of 600–990 nm, the reflection shows a downward trend. Due to the increase of particle size,
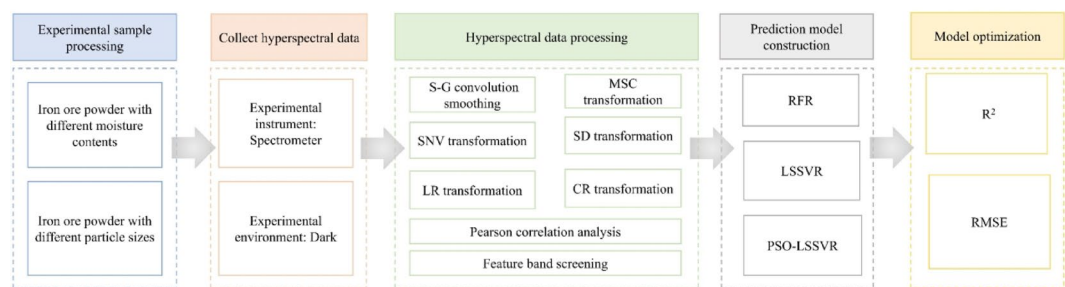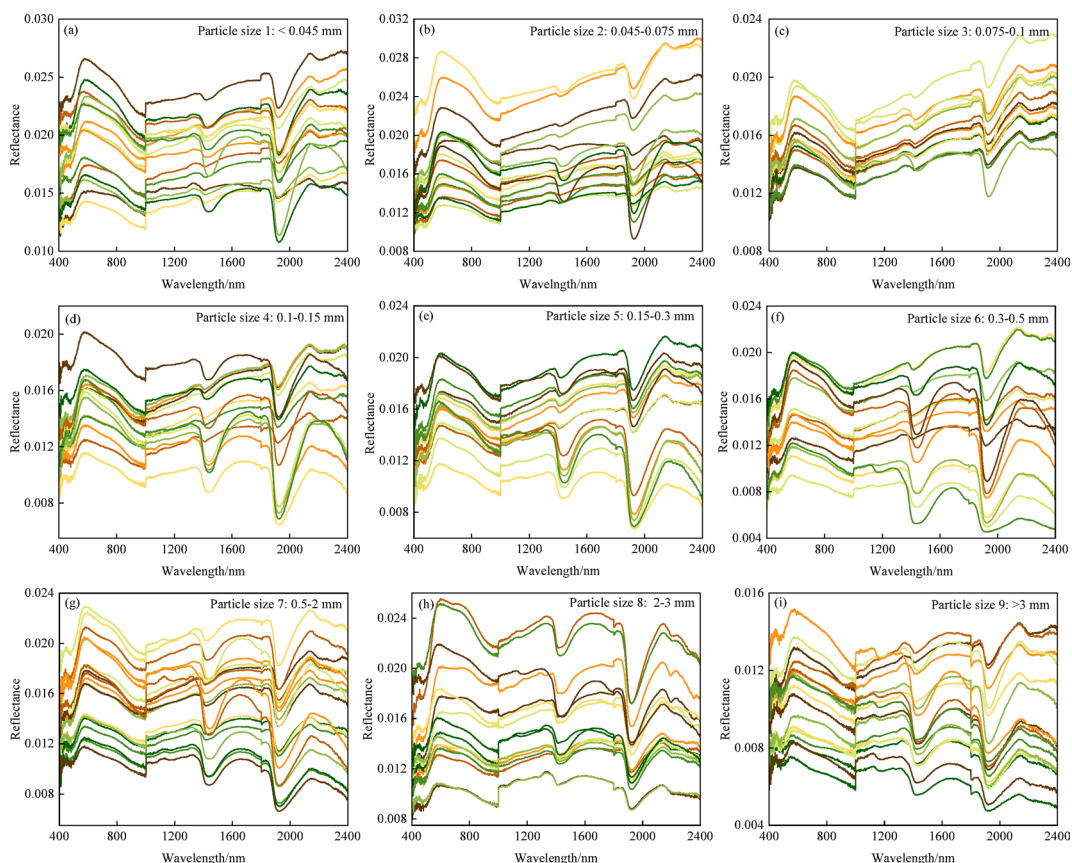
Fig. 2. Methodological flowchart.

Fig. 3. Nine Hyperspectral curves of magnetite with different particle sizes and water contents: (**a**) particle size 1; (**b**) particle size 2; (**c**) particle size 3; (**d**) particle size 4; (**e**) particle size 5; (**f**) particle size 6; (**g**) particle size 7; (**h**) particle size 8; (**i**) particle size 9.

the spectral characteristics of Fe^{3+} are suppressed, and the band of 750–800 nm gradually tends to be flat. The absorption band of Fe^{3+} appears near 990 nm. In the range of 990–1920 nm, the reflectivity is relatively stable, and there are absorption peaks caused by the vibration of -OH bond at 1440 nm and 1920 nm, and the higher the water content, the stronger the absorption depth. The spectral reflectance tends to be stable at 1920–2400 nm. The change of water content of magnetite has little influence on the overall trend of reflection spectrum curve, but it has great influence on the spectral reflectivity. The water content is negatively correlated with the overall reflectivity of magnetite and positively correlated with the absorption depth of characteristic peak.

Correlation analysis results of spectral data preprocessing and pearson

The spectral data of magnetite with nine particle sizes are transformed and the data results are shown in Fig. 4. Compared with the original spectral curve, the 6 spectral transformations enhance the spectral characteristics and remove some noise to a certain extent, and the results of MSC and SD transformation tend to highlight the overall spectral characteristics. Figure 4(a) shows the spectral curve after S-G smoothing, and the curve variation law is almost the same as the original spectral curve, which well preserves the original shape of the
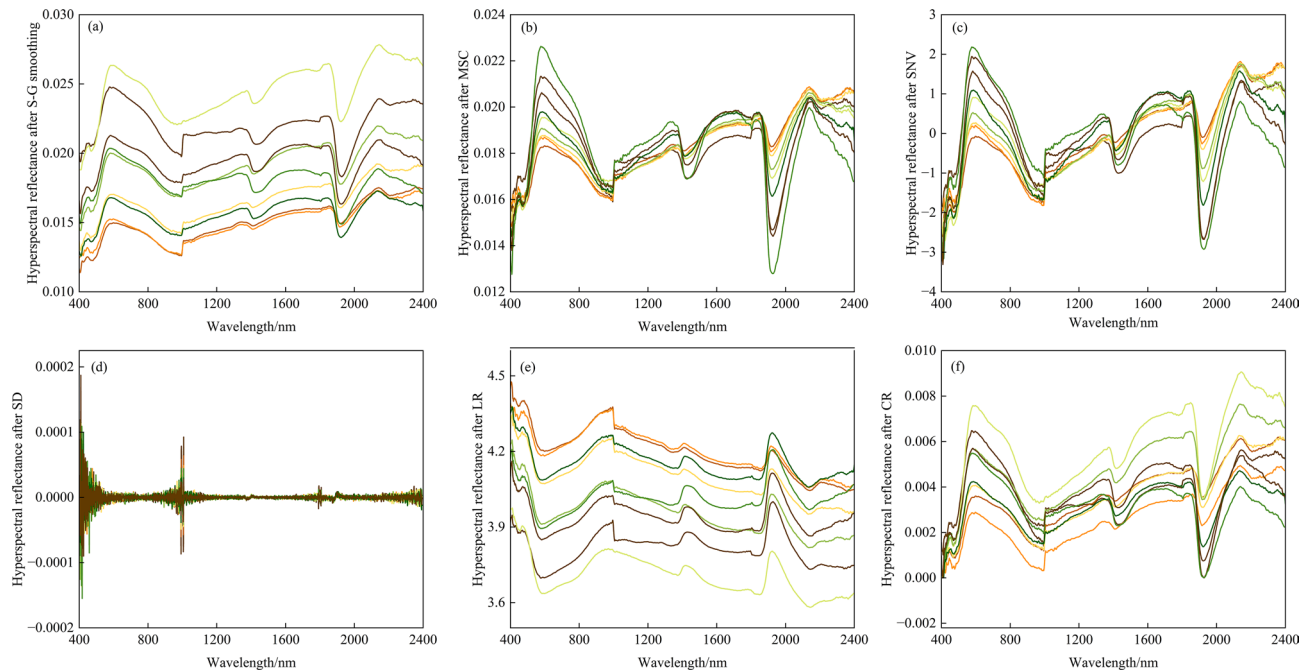
Fig. 4. Spectral data results of 9 kinds of magnetite particles after transformation: (**a**) S-G smooth; (**b**) MSC; (**c**) SNV; (**d**) SD; (**e**) LR; (**f**) CR.

spectrum and has obvious noise filtering effect in the band of 400–550 nm. Figure 4(b) is the spectral curve after MSC transformation, highlighting the absorption characteristics at 1440 nm and 1920 nm, and the absorption depth is positively related to the particle size, which is mainly related to the surface characteristics of particles and the light scattering mechanism. When the particle size is larger, the ratio of its surface area to volume increases, and more light is reflected by the particle surface, and the large particle size usually leads to multiple scattering of light, which increases the ratio of reflected light. Figure 4(c) and Fig. 4(f) are curves after SNV and CR transformation. Compared with other transformations, the spectral characteristics near 440 nm, 990 nm, 1440 nm and 1920 nm are more obvious. Figure 4(d) SD transform has the best spectral features at 440 nm, 990 nm and 1920 nm. With the increase of particle size, the features around 1920 nm are enhanced, but the effect of filtering noise is relatively poor. Figure 4(e) The characteristics of LR transform at 1920 nm are obviously different, and the reflectivity of different water contents is obviously distinguished.

The correlation coefficient between water content and spectral reflectance after different spectral transformations is shown in Fig. 5. The overall change trend of the correlation of the six transformations is consistent, and LR shows a partially opposite trend. After MSC, SNV, LR and CR transform, the correlation of most bands is obviously improved. The absolute value of correlation coefficient between MSC and SNV is about 0.8, that of S-G, LR and CR transform is about 0.6, and that of SD transform is about 0.5. In particle size 1, the maximum correlation coefficients between MSC and SNV are −0.908 (459 nm) and-0.914 (465 nm). The correlation of particle sizes 2, 3, 4, 8 and 9 is low, and the average correlation coefficient is about 0.6. The maximum correlation coefficients of particle sizes 5, 6 and 7 are −0.950 (412 nm), −0.903 (435 nm) and −0.946 (438 nm) in MSC transformation, and −0.892 (457 nm) and −0.902 (492 nm) in SNV transformation, respectively. By comprehensive comparison, MSC and SNV transform have strong adaptability to the spectral data of magnetite water content, and the effect of improving data quality is good.

CARS algorithm feature band screening to improve data quality

With the increase of sampling times, the change results of the number of bands selected by the sample, RMSECV and regression coefficient of each band are shown in Fig. 6. With the increase in Monte Carlo sampling times, there are fewer and fewer remaining variables. In the process of increasing the number of runs, the accuracy of the model will increase with the deletion of useless variables in the early stage, but when the variables decrease in the later stage, the useful variables will also be deleted, leading to the increase of RMSECV. After several runs, the better results will be selected.

The characteristic band positions of six transformed spectral data screened by CARS are shown in Fig. 7. This process effectively reduces the redundancy of the data and provides a more refined database for subsequent analysis. The characteristic bands screened by different transformation methods are different. The bands screened by S-G, MSC, and LR transform are mainly located around 440 nm and 900 nm, while the characteristic bands of SD transform are mainly concentrated in the range of 440–500 nm, and the bands screened by SNV and CR transform are mainly distributed around 400 nm and 1350 nm. Through the screening of the CARS algorithm, the key features of spectral data are highlighted, and redundant information is eliminated, which further
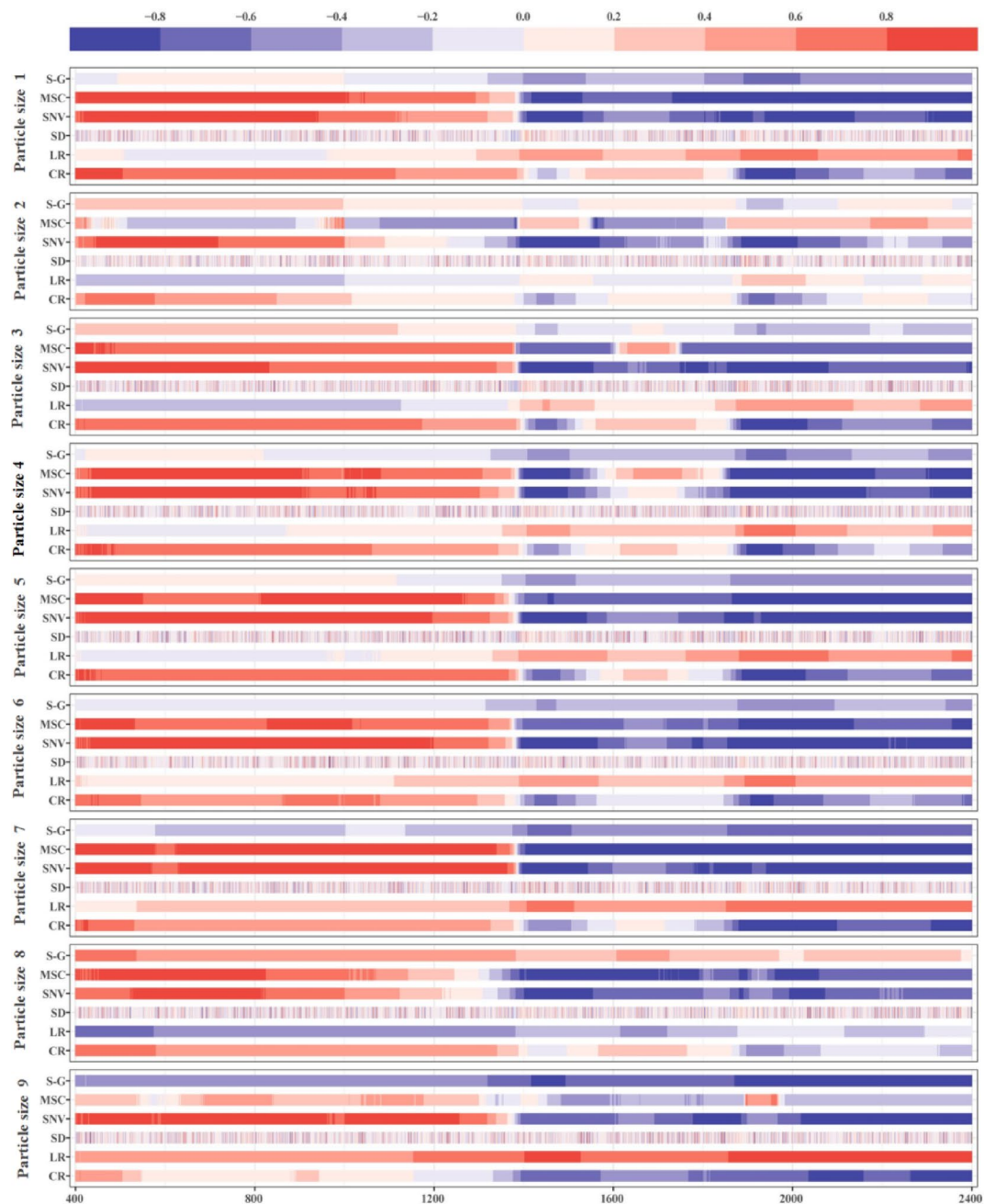
Fig. 5. Thermal diagram of correlation between water content and spectral reflectance after different transformations.
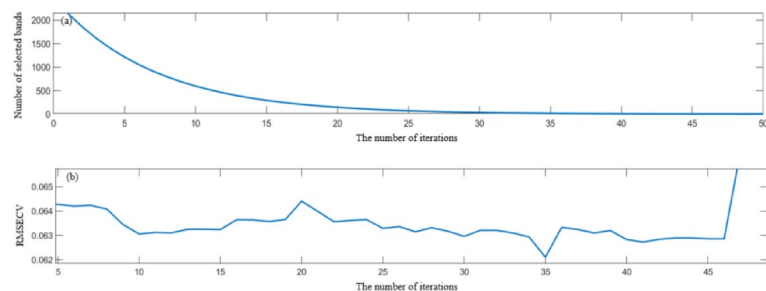

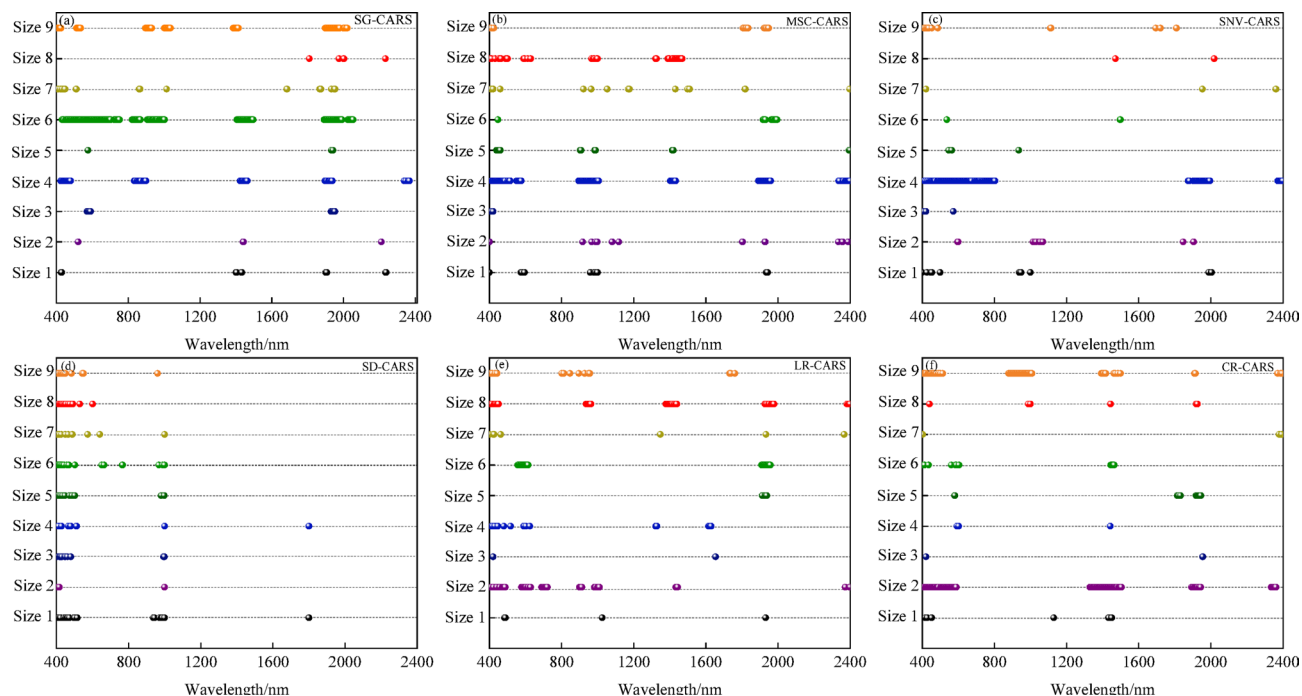**Fig. 6**. CARS screening process: (**a**) Number of selected bands; (**b**) RMSECV.

Fig. 7. CARS algorithm processes the screening results of spectral characteristic bands after pretreatment of 9 particle sizes: (**a**) SG-CARS; (**b**) MSC-CARS; (**c**) SNV-CARS; (**d**) SD-CARS; (**e**) LR-CARS; (**f**) CR-CARS.

improves the quality of spectral data and ensures that the model can capture the spectral information related to water content more accurately, thus improving the accuracy and reliability of prediction.

Establishment and optimization results of water content prediction model

Based on 6 characteristic bands of spectral transformation selected by CARS algorithm, combined with three models of RFR, LSSVR and PSO-LSSVR, the water content of magnetite with nine particle sizes was estimated, resulting in 162 different results. When analyzing these results, it is found that the magnetite powder with particle sizes of 1, 2, 3 and 4 is easy to bond when the water content increases, resulting in relatively poor spectral recognition effect; However, for magnetite with particle sizes of 8 and 9, due to the large surface characteristics of particles and light scattering, the effect of identification model is good but not outstanding. By comparing the prediction effects of all particle sizes, it is found that magnetite with particle sizes of 5, 6 and 7 has the best prediction effects under the three models, indicating that moderate particle sizes are more conducive to improving the accuracy and stability of spectral identification.

Figure 8 is a scatter plot of the predicted value and the measured value of the optimal spectral transformation mode in the three models. Figure 8(a-l) are the optimal results of RF, LSSVR and PSO-LSSVR models respectively. The data points of RF and PSO-LSSVR models are more concentrated and closer to the 1:1 line, while the data points of LSSVR model are more discrete, which may easily lead to data instability. Among the three models, PSO-LSSVR has the most stable model effect, and the training set R^2 reaches about 0.980. Particle size 1(SNV-CARS-PSO-LSSVR), 5(MSC-CARS-PSO-LSSVR), 5(SNV-CARS-PSO-LSSVR), 6(MSC-CARS-PSO-LSSVR) and 7(CR-CARS-PSO-LSSVR). After transformation, the accuracy of the model has been improved to varying degrees, among which MSC, SNV and CR have better effects. In the RF model, the effects of particle size 1(MSC-CARS-RF), particle size 5(MSC-CARS-RF), particle size 6(SNV-CARS-RF) and particle size 7(CR-CARS-RF) are the best, and the prediction sets R2 are 0.547, 0.663, 0.549 and 0.554 respectively. In the LSSVR model, R^2 of the prediction sets of particle size 6(MSC-CARS-LSSVR), particle size 6(SNV-CARS-LSSVR) and particle size 7(CR-CARS-LSSVR) are 0.668, 0.778 and 0.682, and RMSE is 4.91%, 5.45% and 0.682, respectively. Comparing the three models, the effect of LSSVR model is slightly inferior to that of RF model, and PSO-LSSVR model has the best effect, with higher R^2 and lower RMSE.

The water content prediction model R^2 established by Yu et al. for tailings is 0.798, and the root mean square error RMSE is 0.077. Compared with the field measured values, the water-leaving reflectivity of the remote sensing model of heavy metals established by Liang et al.[21] at the wavelength of 350–950 nm is 0.964, and the verification accuracy R^2 of the iron tailings water content model established by Cao et al.[22] is 0.92, and the field verification R^2 reaches 0.79. In this study, the water content models of magnetite with particle size 1(SNV-CARS-PSO-LSSVR) and particle size 7(CR-CARS-PSO-LSSVR) were finally selected, and the prediction set R^2 was 0.798 and 0.789 respectively, and the RMSE was 5.64% and 5.41% respectively.
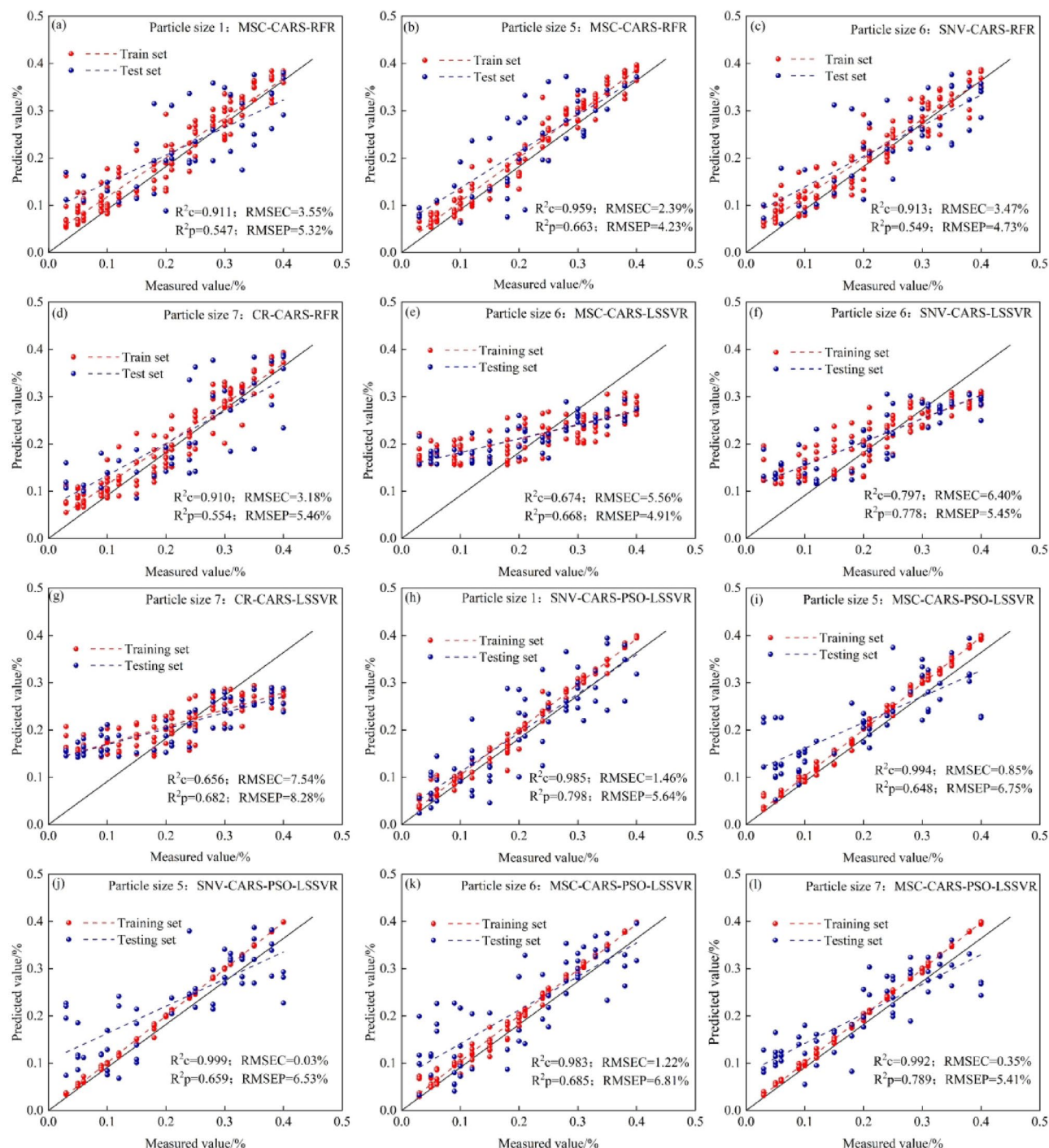
Fig. 8. Results of measured and predicted values of the better model among 9 particle sizes: (**a**-**d**) RF model, (**e**-**g**) LSSVR model; (**h**-**l**) PSO-LSSVR model.

Conclusion

This study investigated nine magnetite samples from Hebei Province with moisture contents ranging from 0 to 40% using hyperspectral techniques. Results demonstrated a clear negative correlation between spectral reflectance and moisture, with prominent absorption features near 990 nm, 1440 nm, and 1920 nm attributed to Fe^{3+} ions and -OH bonds. Advanced preprocessing and feature selection methods effectively enhanced these spectral signatures, reducing noise and improving model inputs. Among the tested models, PSO-LSSVR showed the most stable and accurate moisture predictions across different particle sizes. The selected models achieved high accuracy, providing a reliable method for rapid and precise magnetite moisture detection. This approach offers significant potential for industrial and mining applications, enabling real-time monitoring and improved

process control during ore beneficiation and smelting. Future work will focus on expanding the model to diverse sample types to enhance its generalizability and practical applicability.

Data availability

All data generated or analyzed during this research process are included in this published article.

References

1. Guo, L. J. et al. Research progress on mining with backfill technology of underground metalliferous mine[J]. *J. China Coal Soc.* **47** (12), 4182–4200. https://doi.org/10.3964/j.issn.0253-9933(2022)12-4182-19 (2022).
2. Liu, S. J. et al. Intelligent spectrum sensing technology and research progress of rock and ore in intelligent mine[J]. *Metal Mine.* (7), 1–15. https://doi.org/10.19614/j.cnki.jsks.202107001 (2021).
3. Huang, H. Y. et al. Ground-based hyperspectral inversion of salinization and alkalinization information of different soil layers in farmland in Yinbei area, ningxia, China[J/OL].Chinese journal of applied ecology [2024-09-30]. https://doi.org/10.13287/j.1001-9332.202411.017
4. Wang, Y. C. et al. Study on quantitative inversion of leaf water content of winter wheat based on discrete wavelet technique[J]. *Spectrosc. Spectr. Anal. 2024*, **44**(9):2559–2567. https://doi.org/10.3964/j.issn.1000-0593(2024)09-2559-09
5. Xu, J. et al. Inversion of soil moisture in cotton fields based on UAV hyperspectral remote sensing[J]. *Coal Geol. China 2023*, **35**(08):64–69. https://doi.org/10.3969/j.issn.1674-1803.2023.08.11
6. Wang, Z. G. et al. Hyperspectral inversion study of vertisol soil moisture content based on ensemble learning[J]. *J. Agricultural Resour. Environ.* **40** (6), 1426–1434. https://doi.org/10.13254/j.jare.2023.0186 (2023).
7. Xiong, Y. Q. et al. Direct determination of heavy metals in soil by point discharge atomic emission spectrometry through graphite-doped sample preparation[J]. *Chin. J. Anal. Chem. 2024*, **52**(10):1528–1535. https://doi.org/10.19756/j.issn.0253-3820.241313
8. Liang, Y. J. et al. Multi-star linear regression retrieval model for monitoring soil moisture using GPS-IR[J]. *Acta Geod. Et Cartogr. Sinica 2020*, **49**(7):833842. https://doi.org/10.11947/.AGCS.2020.20190095
9. Wang, D. S. et al. Near-infrared spectral characteristics of sandstone and inversion of water content[J]. *Spectrosc. Spectr. Anal. 2022* **42**(11), 3368–3372 (2022) (**10 3964//j.issn.1000 − 0593(2022)11-3368-05**).
10. Xian, L. H. et al. Estimation models of forest stand biomass using combined multi-spectral and lidar technologies[J]. *J. Northeast Forestry Univ. 2024*, **52**(8):85–94. https://doi.org/10.13759/j.cnki.dlxb.2024.08.010
11. Zhang, F. et al. Comparative analysis of near-infrared spectral characteristics of water-bearing rocks with different lithologies[J]. *Spectrosc. Spectr. Anal. 2020*, **40**(03):971–979. https://doi.org/10.3964/j.issn.1000-0593(2020)03-0971-09
12. Bai, Y. S. & Liu, H. L. Zinc based on spectral feature analysis of geophysical prospecting of mineral reserves evaluation[J]. *World Nonferrous Met.*, **2016**(16):68–69. https://doi.org/10.3964/j.issn.1002-5065(2016)16-0068-2
13. Gao, Y. et al. On-Line analysis of sinter mixture composition and correction of moisture influence based on laser-induced breakdown spectroscopy[J]. *Chin. J. Lasers 2023*, **50**(19):198–206. https://doi.org/10.3788/CJL221270
14. Maurais, J. et al. Monitoring moisture content and evaporation kinetics from mine slurries through albedo measurements to help predict and prevent dust emissions[J]. *Royal Soc. Open. Sci.* **8** (7), 210414 (2021). : 10 3964/j.issn.1000 − 0593(2019)10-3096-06.
15. Li, X. et al. Comparative analysis of hyperspectral Estimation models for soil texture in coastal wetlands[J]. *Spectrosc. Spectr. Anal. 2024*, **44**(9):2568–2576. https://doi.org/10.3964/j.issn.1000-0593(2024)09-2568-09
16. Sun, J. Q. et al. Hyperspectral prediction method for perilla aldehyde content in perilla frutescens[J]. *Spectrosc. Spectr. Anal. 2024*, **44**(09):2667–2674. https://doi.org/10.3964/j.issn.1000-0593(2024)09-2667-08
17. Yuan, J. Q. et al. Early identification of rice panicle blast in canopy based on hyperspectral imaging[J]. Journal of Southwest University (Natural Science Edition), 2023,45(06):57–65. https://doi.org/10.13718/j.cnki.xdzk.2023.06.006
18. Peng, J. N. & Xu, H. Y. Wind power prediction algorithm based on random forest and support vector regression [J]. *J. Eng. Therm. Energy Power 2024*, **39**(05):143–149. https://doi.org/10.16146/j.cnki.rndlgc.2024.05.016
19. DAVOODI, F. et al. A new method for evaluating the bearing capacity of aluminum alloy double-layer coating based on PLS and SVR model [J]. *Trans. Nonferrous Met. Soc. China 2022* **32**(06), 1834–1851 (2022).
20. Liu, B. et al. Performance prediction and optimization strategy for LNG multistage centrifugal pump based on PSO-LSSVR surrogate model[J]. *Cryogenics* **140**, 103856 (2024).
21. Liang, Y. H. et al. Spectral characteristics of sediment reflectance under the background of heavy metal polluted water and analysis of its contribution to water-leaving reflectance[J]. *Spectrosc. Spectr. Anal. 2024*, **44**(1):111–117. https://doi.org/10.3964/j.issn.1000-0593(2024)01-0111-07
22. Cao, Y. et al. Research on remote sensing inversion method of surface moisture content of iron tailings based on measured spectra and domestic Gaofen-5 hyperspectral high-resolution satellites[J]. *Spectrosc. Spectr. Anal. 2023*, **43**(4):1225–1233 .

Acknowledgements

Author contributions

Xiaoxiao Xie: Writing – original draft, Writing – review & editing,Visualization, Validation, Software, Resources, Project administration, Methodology, Investigation, Data curation, Conceptualization. **Yang Bai**: Supervision, Resources, Investigation, Funding acquisition. **Jiuling Zhang**: Supervision, Project administration. **Yuna Jia**: Supervision, Resources, Funding acquisition. **Handi Wang**: Conceptualization, Resources.

Funding

Declarations

Competing interest

The authors declare that they have no known competing financial interests or personal relationships that could

have appeared to influence the work reported in this paper.

Additional information

Correspondence and requests for materials should be addressed to X.X.

Reprints and permissions information is available at www.nature.com/reprints.

Publisher's note Springer Nature remains neutral with regard to jurisdictional claims in published maps and institutional affiliations.